Pharm Res (2013) 30:458–477
DOI 10.1007/s11095-012-0892-4

RESEARCH PAPER

Freeze-Dried Mannitol for Superior Pulmonary Drug Delivery via Dry Powder Inhaler

Waseem Kaialy • Ali Nokhodchi

Received: 19 July 2012 / Accepted: 24 September 2012 / Published online: 16 October 2012

ABSTRACT

Purpose To show for the first time the superior dry powder inhaler (DPI) performance of freeze dried mannitol in comparison to spray dried mannitol and commercial mannitol.

Methods Different mannitol powders were sieved to collect 63–90 μm particles and then analyzed in terms of size, shape, surface morphology, solid state, density, flowability. Salbutamol sulphate-mannitol aerosol formulations were evaluated in terms of homogeneity, SS-mannitol adhesion, and *in vitro* aerosolization performance.

Results Freeze dried mannitol demonstrated superior DPI performance with a fine particle fraction believed to be highest so far reported in literature for salbutamol sulphate under similar protocols (FPF=46.9%). To lesser extent, spray dried mannitol produced better aerosolization performance than commercial mannitol. Freeze dried mannitol demonstrated elongated morphology, α-+β-+δ- polymorphic forms, and poor flowability whereas spray dried mannitol demonstrated spherical morphology, α-+β- polymorphic forms, and excellent flowability. Commercial mannitol demonstrated angular morphology, β- polymorphic form, and good flowability. Freeze dried mannitol demonstrated smoother surface than spray dried mannitol which in turn demonstrated smoother surface than commercial mannitol. FPF of SS increased as mannitol powder porosity increase.

Conclusions Freeze drying under controlled conditions can be used as a potential technique to generate aerodynamically light mannitol particles for superior DPI performance.

KEY WORDS aerosol · freeze dried mannitol · morphology · porosity · spray dried mannitol

INTRODUCTION

Pharmacologically active drugs usually betray poor physicochemical properties and therefore formulation development is often considered challenging. Milling is the most conventional method to prepare particles in the size range between 1 μm and 10 μm which are widely used in chemical, mineral, and pharmaceutical industries (e.g. preparation of respirable aerosol particles). Many mills have been employed for drug micronization such as fluid-energy mills (e.g. the jet mill), high peripheral speed mills (e.g. the pin mill), and ball mills. Jet milling (or air attribution milling) is the most commonly used milling technique. Jet milling depends on introducing pressurized high velocity gas (air or nitrogen) through nozzles into the milling chamber, which results in high-speed (sonic velocities) particle-particle collision (interparticle collision) and abrasion. The efficiency of jet milling is significantly affected by the nature of the particles fed into the jet mill. For example both large and small particles were not ideal for jet milling, and the preferred particle size of most materials for jet milling was in the range of 75 to 100 μm. Also, brittle materials have a tendency to fracture

W. Kaialy (✉) · A. Nokhodchi
Chemistry and Drug Delivery Group, Medway School of Pharmacy
University of Kent
ME4 4TB Kent, UK
e-mail: waseemkaialy@hotmail.co.uk

A. Nokhodchi
e-mail: a.nokhodchi@kent.ac.uk

W. Kaialy
Pharmaceutics and Pharmaceutical Technology Department
University of Damascus
Damascus, Syria

A. Nokhodchi
Drug Applied Research Center and Faculty of Pharmacy
Tabriz University of Medical Sciences
Tabriz, Iran

during jet milling whereas ductile materials (or plastic materials) might undergo plastic deformation rather than fracturing. Despite its popularity, jet milling technique suffers from several disadvantages (extremely inefficient). This could be attributed to poor performance of jet milled products due to several reasons including the low opportunity to control particle physical properties (e.g. size, shape, morphology, and surface texture), reduced crystallinity, poor flowability, high electrostatic charge, high cohesiveness (agglomeration tendency), possible chemical degradation, and safety concerns due to dust exposure (1).

Spray drying (introduced in the 1980s) has been widely used as a micronization technique to produce particles for pulmonary delivery (2). In pharmaceutical industry, spray drying is the most commonly used technique in preparing peptides and proteins for inhalation as a dry powder. Nevertheless, spray drying technique suffer from several disadvantages such as reduced crystallinity for spray dried products, not suitable for substances susceptible to atomization mechanical shear (e.g. biopharmaceutical drugs), not suitable for substances that are unstable to liquid–air interface or decomposed by oxidation, and very low process yield. Anti-solvent crystallization is a process where, generally, an organic product can be recovered from aqueous solutions through the addition of nonsolvent compounds by which the solute solubility is decreased without creating a new liquid phase. Recently, anti-solvent crystallisation using binary nonsolvents was proved to be potential method to prepare mannitol (3,4) and lactose (5–7) particles with superior dry powder inhaler (DPI) performance. However, anti-solvent crystallisation using alcohols suffer from many disadvantages including the requirement of solvent recovery and the risk associated with the use of flammable solvents at high reaction temperatures. Also, mechanical stirring used during crystallization introduces random energy fluctuations with the solution leading to heterogeneous distribution of local concentrations and consequently heterogamous crystal growth. Freeze drying is a technique by which it is possible to recover dry product from aqueous solutions. Commonly, freeze drying is used for preparing injectable pharmaceutical products.

After 20 years of using metered dose inhalers (MDIs), the first DPI was introduced to the market at 1970 (Fisons, Spinhaler®). In literature, it has been shown that it is possible to obtain increased respirable drug fraction by decreasing particle size of carrier particles (8,9). However, other reports showed that carrier particle mean diameter has no effect on aerodynamic diameter (10) or on fine particle fraction of drug (11). Furthermore, other reports showed that larger carrier particles might outperform smaller carrier particles (12,13). In comparison to control, carrier particles with more elongated shape (3,4,14,15) or less elongated shape (6–8) deposited higher amounts of drug on lower airway regions. Generally, no significant relationship was observed between FPF of drug and flowability of carrier powder (8). Better aerosolization performance was obtained from DPI formulations with either better flow properties (16) or poorer flow properties (3,4). Such apparently dissimilar results could be explained as the physical properties determinations of carrier particles are dependent on each other, and to the fact that DPI aerosolization behaviour is reliant on several interrelated events at the same time. For example, it was shown that, in determining DPI performance, carrier polymorphic form and surface energy dominates over carrier size distribution (17). Also, type of drug (18), type of inhaler device (19), amounts of fine carrier particles (20), and carrier surface texture (21) may have an effect on the preferable carrier size for enhanced aerosolisation performance. For example, In case of DPI formulation powders containing coarse carrier particles, higher respirable fractions were obtained when using high-efficiency dispersing systems (high turbulence inhalers). However, for DPI formulations containing carriers with large amount of fine particles, effective dispersion was obtained when using low turbulent inhaler devices.

Lactose has some degree of security when it is used as inert excipient considering its incompatibility with drugs that have primary amine moieties making it less suitable excipient for next generation of inhalable products (i.e. proteins and peptides). Therefore, using alternative excipients appears to be an attractive option for DPI formulations. Possible excipients for dry powder inhalation formulations are rather narrow as they have to meet specific conditions such as being endogenous, able to be metabolised or cleared, and have no potential to injure or irritate the lungs. Therefore, in inhalation field, only generally recognized as safe (GRAS) excipients can be used. Mannitol was attractive alternative since it does not have a reducing effect, less hygroscopic, and gives high sweet aftertaste which could be used to observe dose taken by the patient. Also, mannitol is the most abundant polyol in nature, has been used widely for commercial pharmaceutical protein formulations due to its biological stabilizing efficiency properties, is the most widely used bulking agent in freeze dried formulations, and is expected to be approved in future for use of DPIs (22). This is because of mannitol is inert, has good cake-supporting properties, crystallises readily during freeze drying, and allows drying processed at higher product temperatures (23). Mannitol is a polyol cryoprotectant and a lyoprotectant that lead to crystalline freeze dried systems (24). The mannitol/ice eutectic mixture has a high melting temperature ($\sim -1.5°C$) promoting efficient freeze drying and physical stability of freeze dried mannitol solid (25).

Despite over 40 years of research, low drug delivery efficiency to the lower airway regions is still a major challenge for dry powder aerosol pharmaceutical dosage forms

(8). In pharmaceutical industry, there is increased interest for pharmaceutical excipients, other than lactose, which produce efficient drug delivery upon inhalation. The objective of this study was to introduce, for the first time, freeze dried mannitol as alternative promising carrier in DPI formulations containing salbutamol sulphate as a model drug. Also, this study was performed with a view to propose optimal mannitol product (freeze dried mannitol *vs* spray dried mannitol *vs* commercial mannitol) for salbutamol sulphate based drug-carrier dry powder inhaler formulations. It was intended in this study to show how different mannitol grades perform inherently under similar protocols including blending and sieving.

MATERIALS AND METHODS

Materials

Commercial mannitol (CM) (Fisher Scientific, UK) and spray dried mannitol (SDM) (SPI Pharma, UK) were purchased from the named sources. Micronized salbutamol sulphate (SS, $D_{10\%}$=0.5±0.0 μm, $D_{50\%}$=1.7±0.1 μm, $D_{90\%}$=3.1±0.3 μm (3)) was supplied from LB Bohle, Germany.

Preparation of Freeze-Dried Mannitol (FDM)

Mannitol was freeze dried using a SCANVAC CoolSafe™ freeze-dryer (CoolSafe 110-4, Lynge, Denmark). A 5% *w/v* mannitol solution was prepared by dissolving 5 g of mannitol in distilled water such that the final solution volume is 100 mL. 100 mL of mannitol solution was filled into 250 mL round-bottomed flask and left in freezer overnight after which it was placed on the shelves of the freeze-dryer. Samples were freeze dried at −110°C and collected after 48 h after which they were transferred into sealed glass vials over silica gel until used.

Sieving

In order to limit the influence of mannitol particle size on aerosolization performance, similar size fraction (63–90 μm) of each mannitol powder was used. Mechanical sieving was applied via mechanical shaker (Endecotts Ltd, England) as described in details elsewhere (3).

Particle Size Measurements

Particle size analysis was carried out using a Sympatec (Clausthal-Zellerfeld, Germany) laser diffraction particle size analyser as described in details elsewhere (4). The span (calculated from Eq. (1)) of the volume distribution was used as a measure of the width of the distribution relative to the median diameter:

$$Span = \frac{d[v,90] - d[v,10]}{d[v,50]} \quad (1)$$

Image Analysis Optical Microscopy

Quantitative particle shape analysis was conducted using a computerized morphometric image analyzing system (Leica DMLA Microscope; Leica Microsystems Wetzlar GmbH, Wetzlar, Germany; Leica Q Win Standard Analyzing Software) as explained in details elsewhere (26,27). In order to get good understanding of particle morphology, several shape factors have been applied as none of these descriptors is able to accurately differentiate between geometric shape and surface roughness. Particle shape were quantified using several descriptors including aspect ratio (Eq. 2), flakiness ratio (Eq. 3), sphericity (Eq. 4), compactness (Eq. 5), and simplified shape factor (Eq. 6) as defined elsewhere (26–28)

$$Aspect\ ratio = \frac{Length}{Breadth} \quad (2)$$

$$Flakiness\ ratio = \frac{Breadth}{Thickness} \quad (3)$$

$$Sphericity = \sqrt[3]{\frac{Width \times Thickness}{(Length)^2}} \quad (4)$$

$$Compactness = \frac{(Perimeter)^2}{Area} \quad (5)$$

$$Simplified\ shape\ factor = \frac{Perimeter_{convex}}{Perimeter} - \sqrt{1 - \left(\frac{breadth}{length}\right)^2} \quad (6)$$

Aspect ratio and flakiness ratio (flatness ratio) are the fundamental first order shape descriptor of a particle. Regardless of orientation, a perfect sphere is expected to have an aspect ratio and flakiness ratio of 1 whereas non-spherical particle will have an aspect ratio and flakiness ratio of <1 or >1. Higher aspect ratio indicates more elongated shape and/or rougher surface whereas higher flakiness ratio indicates flatter particles. As sphere is the simplest dimensional shape, shape of solid particles is frequently described by their Sphericity. Sphericity shape parameter is a descriptor of how a

particle is similar to sphere. A typical smooth sphere is expected to have a sphericity value of unity. A sphere particle with measurable surface asperities or non-spherical particle will have a sphericity value <1. Smaller sphericity values indicate higher degree of shape irregularity and/or higher surface roughness. Compactness is a measure of how nearly circular an aggregate cross section is (27).

Scanning Electron Microscope (SEM)

Electron micrographs of different mannitol samples were obtained using a scanning electron microscope (HITACHI SU 8036, Japan) operating at 5–15 kV as explained in Kaialy *et al.* (26).

Atomic Force Microscope (AFM)

Atomic force microscopy analysis were as performed using a Veeco MultiMode AFM equipped with an E-type scanner operating via a Veeco Nanoscope IIIa controller (Bruker AXS Inc., Bruker Nano Surfaces, Madison, WI, USA) as described in details elsewhere (4). Roughness analysis was performed using Veeco Nanoscope software (version 5.12b36) on images of 5×5 μm^2 and 300×300 nm^2 sized.

Differential Scanning Calorimetry (DSC)

A differential scanning calorimeter (DSC7, Mettler Toledo, Switzerland) was used to characterise solid state nature of different mannitol samples, as described previously (26).

Fourier Transform Infrared Spectroscopy (FT-IR)

FT-IR was employed to give investigate any chemical changes at molecular level in freeze dried mannitol and spray dried mannitol samples in comparison to commercial mannitol. The method incorporated was adapted from Kaialy *et al.* (27).

Powder X-ray Diffraction (PXRD)

The patterns of all mannitol samples were collected on a Bruker D8 Advance Siemens powder diffractometer with Cu Kα radiation (1.54056 Å) using the DIFFRACplus software, as explained in Kaialy *et al.* (14). Quantitative mannitol crystal form analysis (% α-, % β-, or % δ-mannitol) were performed by Rietveld refinement using Topas v4 (Bruker). Cif structural models (adapted from Fronczek *et al.* (29)) of mannitol polymorphs were obtained from the Cambridge Structural Database and refined within Topas on pure mannitol samples and then converted to str files. All refinements were done using fundamental parameters routine based on the configuration of our diffractometer.

Particle True Density Measurements

True density of all mannitol particles (defined as particle mass divided by its volume excluding both open pores and closed pores) was measured using an ultrapycnometer 1,000 according to Kaialy *et al.* (27).

Characterization of Powder Bulk and Flow Properties

Bulk density, tap density, and porosity (Eq. 7) of each mannitol powder sample were measured as important descriptors of powder bulk cohesive properties. Carr's index (CI, Eq. 8) was measured for all mannitol powders to characterize flowability of mannitol powders. The method incorporated was described elsewhere (14)

$$Porosity = \left(1 - \frac{Bulk\ density}{True\ density}\right) \times 100 \tag{7}$$

$$CI = \left(\frac{Tap\ density\_Bulk\ density}{Bulk\ density}\right) \times 100 \tag{8}$$

Preparation of SS-Mannitol Formulations

Each mannitol powder (3 g) was blended with SS powder at a constant ratio of mannitol: SS 67.5: 1, *w/w* which is the same ratio used in commercially available Ventolin Rotacaps®. This blending was performed in a cylindrical aluminium container (6.5×8 cm) using a Turbula® mixer (Maschinenfabrik, Basel Switzerland) at a standard mixing conditions (100 rpm mixing speed and 30 min mixing time). Once prepared, all formulations were stored in firmly sealed vials over silica gel for minimum 24 h before any investigation to allow any electrical charge relaxation to occur. In order to prepare ordered mixtures of two fine particles, a mixer producing high shear forces would be favorable. However, in this study, a turbulent tumbling mixer (TTM, Turbula®) was used since TTM mixers are usually recommended to produce drug-carrier ordered mixtures in the case of formulations containing one coarse particle component (e.g. mannitol) and one fine particle component (e.g. salbutamol sulphate).

Homogeneity Assessment of SS-Mannitol Formulations

After blending, seven randomly selected samples were taken from different spots of each formulation powder for quantification of SS content. Each sample weighs 33±1.5 mg (which is equivalent to a unit dose of SS: 481±22 μg, in accordance with Ventolin Rotacaps®) and was dissolved in 100 mL distilled water in a volumetric flask. SS was analysed using an HPLC method adapted from Kaialy *et al.* (3). For each formulation, % potency was calculated as the percent amounts of SS to the nominal dose while the degree of SS content homogeneity was expressed in terms of percent coefficient of variation (% CV). % CV of 6% or less was considered as sufficient uniform for DPI.

SS-Mannitol Adhesion Assessments

Air jet sieving with a 20 μm sieve was used to indirectly assess drug-carrier adhesive forces of within all formulations (7,26,27) as described elsewhere (27).

In Vitro Aerosolisation Study

Each formulation was filled manually into hard gelatine capsules (size 3) with 33±1.5 mg powder. Prior to any investigation, all filled capsules were stored in sealed glass vials for at least 24 h in order to allow any charge-dissipation to occur. Deposition profiles of all formulations were assessed *in vitro* (Aerolizer® inhaler device with Multi stage Liquid Impinger (MsLI)), as described in pharmacopoeia and adopted from Kaialy *et al.* (3). Every deposition experiment involved the actuation of ten capsules and was repeated three times. Several parameters were employed to quantify SS deposition profiles from each formulation including recovered dose (RD), emitted dose (ED), mass median aerodynamic diameter (MMAD), geometric standard deviation (GSD), fine particle dose ($FPD_{\leq 5\mu m}$), impaction loss (IL), fine particle fraction ($FPF_{\leq 5\mu m}$, % RD), and dispersibility (DS), as defined elsewhere (3,6). The RD is the sum of the weights of drug (μg) recovered from inhaler device with its fitted mouthpiece adaptor (I+M), induction port (IP), and all stages of the impactor. The emitted dose (ED) is the amount of drug delivered from the inhaler device, which is collected in the induction port and all stages of the impactor (i.e. total RD except for the inhaler device with mouthpiece adaptor). The impaction loss was calculated as the sum of drug amounts collected from the induction port and stage 1 of the MSLI expressed as a percentage to the recovered dose. The percent total recovery (% recovery) was calculated as the ratio of the RD to the theoretical dose (481 μg). Theoretical aerodynamic diameter of mannitol particles were estimated from mannitol volume mean diameter (VMD) and tapped density (ρ) using Eq. 9 (30–32)

$$TAD = VMD\left(\frac{\rho}{\rho_1}\right)^{\frac{1}{2}} \tag{9}$$

where $\rho_1 = 1\ g/cm^3$.

Statistical Analysis

One way analysis of variance (ANOVA) and Tukey's Honestly Significant Difference (HSD) (14,26) test was applied to statistically compare mean results in this study.

RESULTS AND DISCUSSION

Particle Size Distribution (PSD)

Laser diffraction analysis for different mannitol powders showed sigmodial (unimodally distributed) size distributions with most particles falling into the nominal sieve mesh size ranges (Fig. 1a). Despite that all mannitol powders were carefully sieved under similar protocols, CM demonstrated higher volume mean diameter (VMD=108.1±1.6 μm) than SDM (81.4±0.9 μm) and FDM (81.0±0.5 μm) (Fig. 1b). Particle size data were supported by representative photograph images (Fig. 1c–e). In DPI systems, differences in size of carrier particles could have a considerable effect on DPI performance. For example, it has been shown that carriers with smaller size have increased disorder in crystal lattice and improved aerosolization performance (8,9). Unlike CM and SDM samples, where sieving was efficient to remove all particles smaller than 5 μm ($FPM_{<5\mu m}$) and 10 μm ($FPM_{<10\mu m}$) (Fig. 1a, c, d), FDM contained 2.0±0.3% and 3.9±0.6% (*v*/*v*) of $FPM_{<5\mu m}$ and $FPM_{<10\mu m}$ respectively (Fig. 1a) which is also confirmed by microscopic image of FDM (Fig. 1e). Amounts of fines in FDM sample correspond to intrinsic fine mannitol particles which could not be isolated by sieving. FDM demonstrated wider (more heterogeneous) size distribution (span=1.4±0.0, skewness=1.7) in comparison to CM (span=0.8±0.0, skewness=1.4) and SDM (span=0.7±0.1, skewness=1.0) (Fig. 1a, b), which could be also substantiated by the representative photographs for CM, SDM, and FDM (Fig. 1c–e). PSD polydispersity is important in terms of aerosol quality and efficiency since differences in aerosol particle size might lead to differences in lung deposition regions (9).

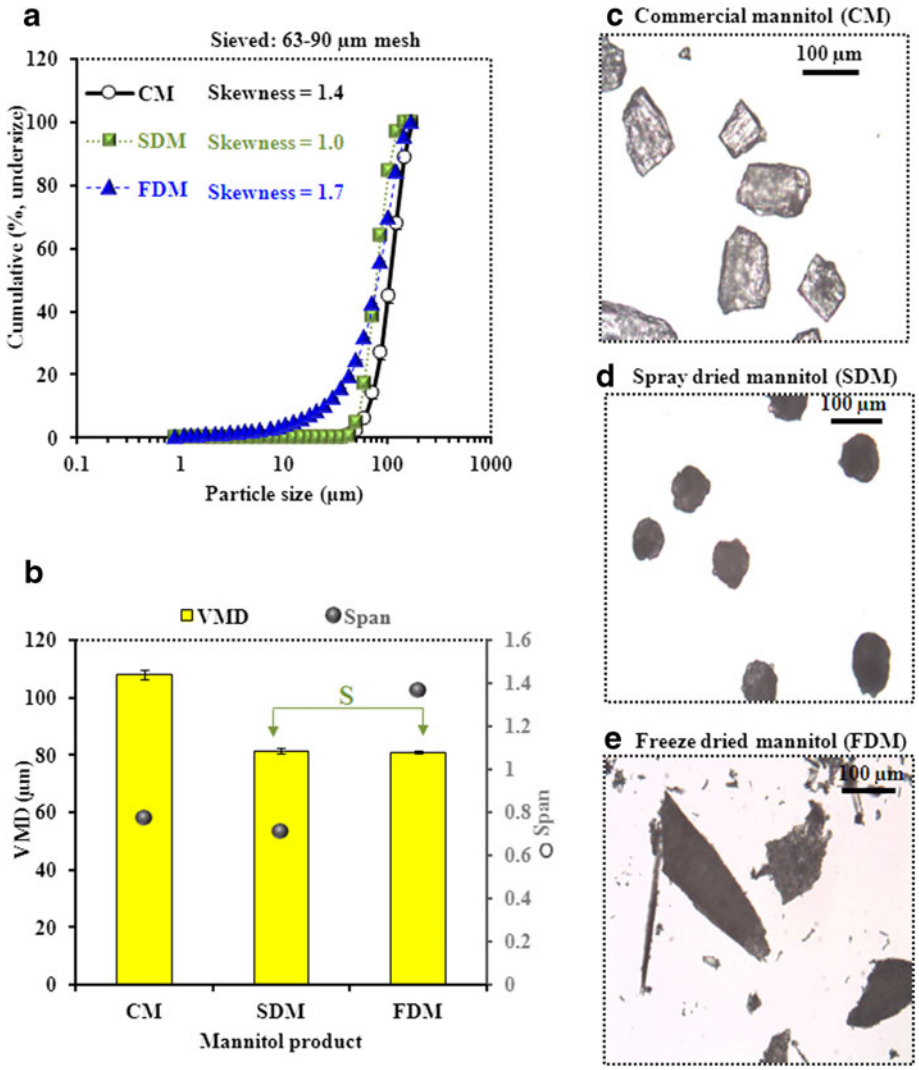

Fig. 1 Particle size distribution (% undersize) (**a**); volume mean diameter (VMD), (*Balck Circle*) span (**b**); and representative photographs for commercial mannitol (CM) (**c**); spray dried mannitol (SDM) (**d**); and freeze dried mannitol (FDM) (**e**). (mean±SD, $n=8$). *S* indicates statistically similar.

Image Analysis Optical Microscopy

Aspect ratio for different mannitol samples was within the following rank order: SDM (1.28±0.0)<CM (1.87±0.01)< FDM (2.54±0.03) (Fig. 2a). In contrary, flakiness ratio for different mannitol samples was within the following rank order SDM (0.89±0.00)>CM (0.73±0.00)>FDM (0.64±0.01) (Fig. 2a). This indicates that, among all mannitol particles, SDM particles have the least elongated-most flattened particle shape, whereas FDM particles have the highest degree of shape-elongation. Such results indicate that, during freeze drying, mannitol crystals grow faster along their length face than along their width. Spherecity for different mannitol samples was within the following rank order: SDM (0.93±0.00)> CM (0.86±0.00)>FDM (0.82±0.00) (Fig. 2b). In contrary, compactness for different mannitol samples was within the following rank order SDM (18.8±0.29)<CM (98.8±2.13)< FDM (103.0±2.73) (Fig. 2a). This indicates that SDM particles have the most spherical-regular morphology whereas FDM particles have the highest degree of shape irregularity. A simplified shape factor was used to estimate the combination of variation in surface asperities (surface texture factor) and deviation of shape from a circle (shape factor) (26,27). This factor is helpful in 2D or 3D shape assessment and can have values from -1 to 1: the smaller the value the more irregular the particle morphology. SDM sample exhibited the highest simplified shape factor (0.29±0.00) whereas FDM sample showed the lowest simplified shape factor (−0.20±0.00).

Such results indicate that SDM proved nearly circular regular-shaped particles whereas FDM showed the most elongated- most irregular-shaped particles. Such information provided by image analysis is compatible with representative photographs of SDM (Fig. 1d) and FDM (Fig. 1e).

Scanning Electron Microscopy

Since the accuracy of particle image analysis data is hindered by particle orientation and interparticulate contact area (7), and therefore might not be satisfactory to represent the influence of particle shape, all mannitol carrier particles

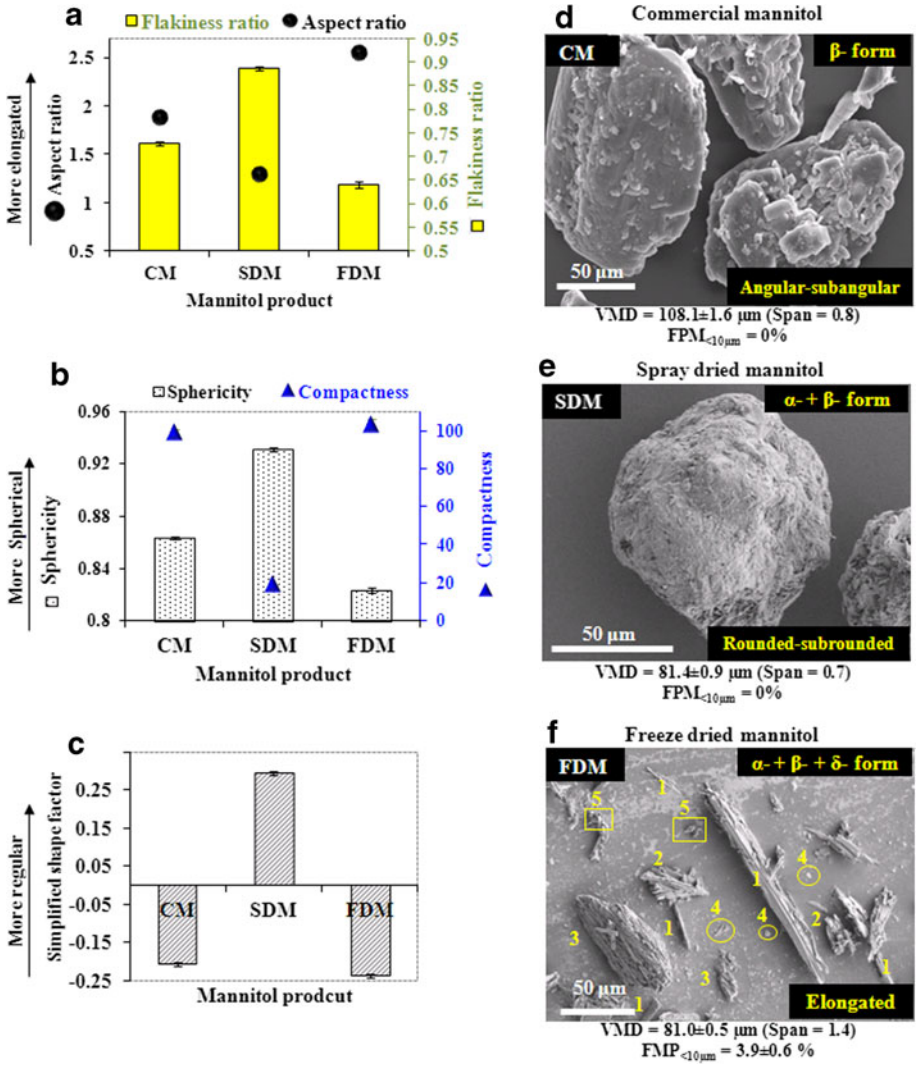

Fig. 2 Aspect ratio (*Black Circle*), flakiness ratio (*Yellow Square*) (**a**); Sphericity (*White Square*), Compactness (*Green Triangle*) (**b**); simplified shape factor (**c**) (mean ± SE, $n \geq 1000$); and representative scanning electron micrographs of commercial mannitol (CM) (**d**); spray dried mannitol (SDM) (**e**); and freeze dried mannitol (FDM); 1: needle shaped, 2: dendritic shaped, 3: dragon like shape, 4: fine particulates ($FPM_{<10\mu m}$), 5: fine particle aggregates (FPA) (**f**).

were further qualitatively analyzed by SEM (Fig. 2d–f). SEM images of different mannitol particles revealed crystalline particles with size typically in 63–90 µm range (supporting laser diffraction data (Fig. 1a)). Strike morphological differences were observed between different mannitol particles (Fig. 2d–f).

CM exhibited the typical angular-subangular shape reported in previous studies. Representative SEM image of SDM illustrated spherical (rounded-subrounded, orange-like) particles with relatively uniform (regular) shape, well curved-plane sides, and well rounded corners and edges (Fig. 2e). No evidence of particle agglomeration was observed in case of CM and SDM samples (Figs. 1c, d, 2d, e). SEM image of FDM revealed irregular-deformed particles with sharp edges and mostly elongated morphology (Fig. 2f). It was clear that, in comparison to CM and SDM, FDM particles are less uniform in terms of shape and size, since several morphologies could be detected: needle shape, dendritic shape (acicular crystals), and dragon like shape (Fig. 2f). Also, finer particulates ($FPM_{<10\mu m}$) and fine particle agglomerates (clusters or microcrystalline assemblies) (FPA) could be depicted in case of FDM sample (Fig. 2f). This supports boarder size distribution (higher span value) for FDM sample as analysed by laser diffraction (Fig. 1b). It was assumed that, during freeze drying, several nucleation points might form resulting in relatively heterogeneous crystal growth and consequently forming particles with different sizes and morphologies.

Higher amounts of fines in case of FDM could be attributed to their brittle properties as indicated by their elongated-irregular morphology and the presence of large number of fractured faces (Fig. 2f). This could promote particle attrition (abrasion or fracturing of cleavage plans) upon subjecting the powder to mechanical sieving process due to inter-particle and particle-sieve wall collisions (27). It can be assumed that, due to low mannitol concentration used during crystallisation (5% *w/v*), crystal growth of FDM crystals was favoured in direction perpendicular to the c-axis (polar growth direction) but less dominant on crystal faces normal to c-axis leading to the formation of elongated crystals.

Variations in morphology of carrier particles have a dominating influence on DPI aerosolization behaviour (14). For example, carrier particles with higher elongation ratio demonstrated smaller surface free energy (33) and improved aerosolization efficiency (3,4). Particles with different shapes will have different drag forces and terminal velocities during aerosolization which in turn affect particle aerodynamic diameter and consequently affect particle deposition profiles in the respiratory airways.

Particle Surface Analysis

Surface morphology of different mannitol particles were visualised from there SE micrographs (Fig. 3a–c). All mannitol particles showed unpolished surfaces (Fig. 3a–c). CM particles showed uneven wrinkled (rough) surface topography with much fragmentation and easily visible cavities (Fig. 3a). SDM particle surface constituted of curved plates of microscopic thickness producing some irregularities in particle surface topography (Fig. 3b). FDM particles exhibited relatively laminated (conchoidal or waterworn-like) smoother surface morphology (Fig. 3c).

At the magnification used for SEM images, nanoscopic indentations might not be visible. Therefore, surface topography of different mannitol particles was analysed by AFM and the representative topographical, amplitude, and phase images are shown in Fig. 3d–i. To investigate the nature of different mannitol surface regions, series of high-resolution (5 μm × 5 μm and 300 nm × 300 nm scan size) AFM images were taken. AFM showed that CM particle has large asperities and protuberances on its surface forming angular edges with signs of cracking (Fig. 3d, g, j). In comparison to CM (Fig. 3a, d), the surface of SDM is flatter, (Fig. 3). This is expected to decrease the number of drug particles remaining in macroscopic surface depressions of mannitol carrier particles and consequently might facilitate drug detachment from carrier surface upon inhalation (3,4,14). Observations of amplitude and phase response suggested the presence of regions with different physico-mechanical properties and thus demonstrated that the method used for preparation of CM sample had a remarkable effect on surface features of CM particles (Fig. 3g, j). These regions could be related to clefts and pits (craters) on the surface of CM particle induced by powder preparation technique. The AFM image of SDM (Fig. 3e, h, k) revealed less corrugated terrace compared to CM (Fig. 3d, g, j). The amplitude/phase images of SDM sample suggested a relatively ordered crystalline state where multiple platelets could be seen across the surface (Fig. 3h, k). The approximate height between platelet steps was around 1–2 μm (Fig. 3e, h, k). Analysis of the amplitude and phase lag information for the FDM sample indicated reduced variation in phase suggesting reduced variation in physicochemical property across the surface (Fig. 3i, l). These results demonstrate that freeze drying process induced relatively ordered crystalline lattice with less changes to the surface in comparison to the method used in preparation of CM sample (and to a lesser extent in comparison to spray drying) which induced disruption of the crystalline lattice.

Roughness analysis (5 × 5 μm) confirmed that CM particles (Rq = 300.1 ± 37.9 nm, Ra = 220.0 ± 17.4 nm) have relatively rougher surfaces than SDM particles (Rq = 189.5 ± 17.6 nm, Ra = 157.2 ± 13.9 nm) which in turn demonstrated quantitatively rougher surface than FDM particles (Rq = 14.2 ± 10.3 nm, Ra = 8.7 ± 1.9 nm) (Fig. 3m). Similar conclusions could be indicated when considering roughness analysis on 300 × 300 nm mannitol region images (Fig. 3n). It was assumed that the relatively low concentration of mannitol used during freeze drying (5% *w/v*) promotes slow kinetics of crystallization and thus slow the crystal growth process resulting in regular growth pattern and consequently generating near-ideal lattices with relatively sufficient time to fill or cover imperfect lattice layers (less "lattice mistakes"). In DPI systems, particle surface roughness affects the contact geometry between the drug and carrier particles and consequently might have a significant impact on drug-carrier adhesion (27).

Particle size and shape determinations are dependent on each other (14). Laser diffraction takes into account the lights diffracted from the dispersed particles to measure particle size, but does not take into account apparent particle density and dynamic shape factors. Therefore, particle size measurements is dependent on particle morphology and orientation (particle morphology information is averaged out to provide one-dimensional distribution during measurement). Angular-corrugated morphology of CM particles (Figs. 2d, 3a) could promote high-angle scattering as measured by laser diffraction and consequently might contribute to larger estimated particle size for CM sample (Fig. 1a) (7).

Solid State Characterization

All mannitol samples produced comparable DSC traces having one endothermic transition at 168.6 ± 1.2°C (Fig. 4) corresponding to α-mannitol or β-mannitol melting (fusion) (Table I). However, FDM showed additional endothermic event at 153.6 ± 0.5°C (Fig. 4) which is diagnostic to melting of δ-mannitol phase followed by the solidification of the melt to form α- or β- polymorph (Table I). Melting enthalpy for different mannitol samples at 168.6 ± 1.2°C was within the following rank order: CM (315.3 ± 10.7 J/g) > SDM (292.5 ± 4.2 J/g) > FDM (257.0 ± 5.6 J/g) (Fig. 4).

All mannitol products did not show any endotherm below 100°C suggesting that they contain a negligible amount of free water (surface water). Also, this suggests the absence

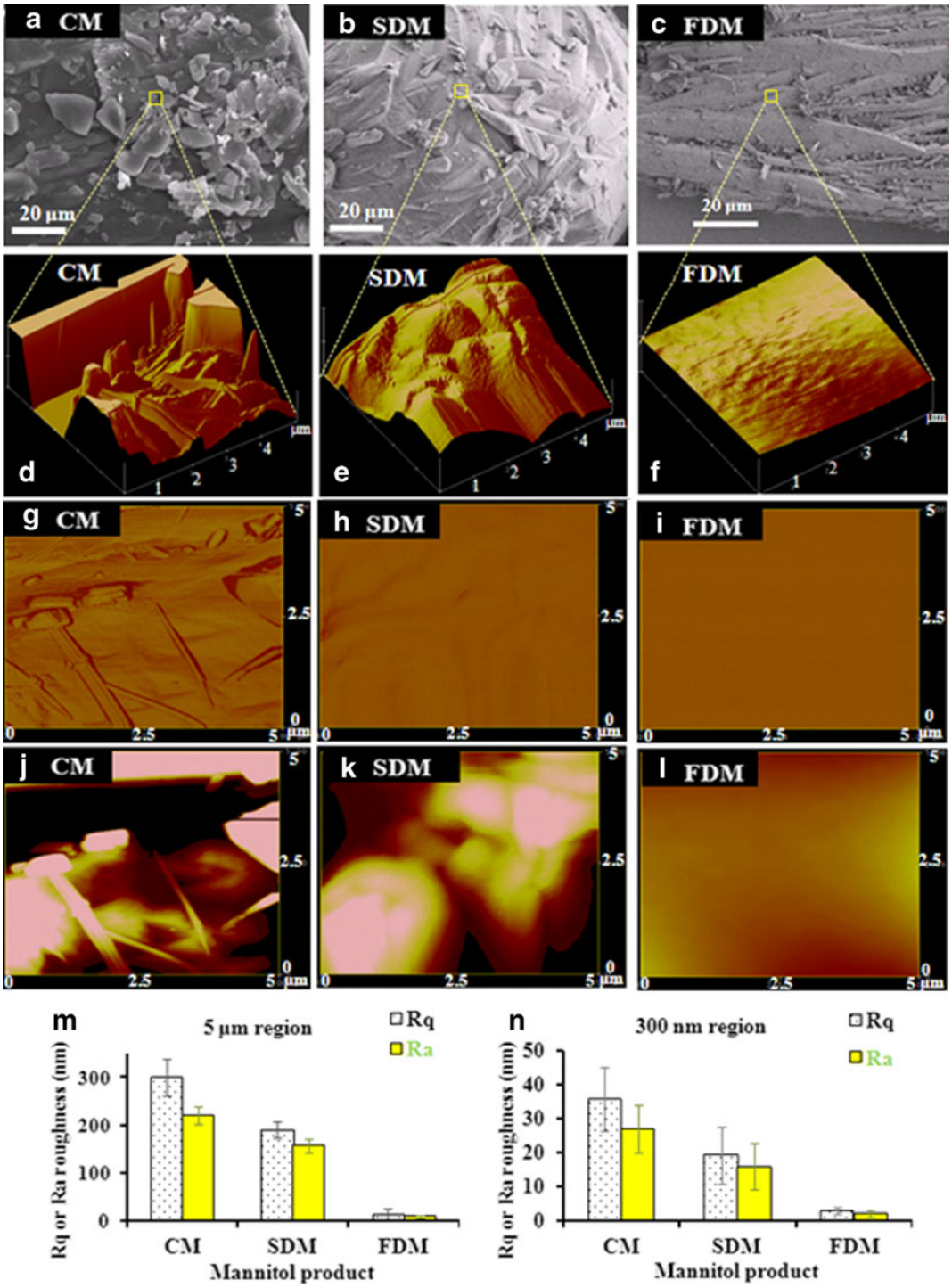

Fig. 3 SE micrographs of commercial mannitol (CM) (**a**); spray dried mannitol (SDM) (**b**); and freeze dried mannitol (FDM) (**c**); topographical AFM image of commercial mannitol (CM) (**d**); spray dried mannitol (**e**); and freeze dried mannitol (**f**); amplitude AFM images of commercial mannitol (CM) (**g**); spray dried mannitol (**h**); and freeze dried mannitol (**i**); phase AFM images of commercial mannitol (CM) (**j**); spray dried mannitol (**k**); and freeze dried mannitol (**l**); root mean square average (Rq) and arithmetic mean average (Ra) roughness on a 5 μm region (**m**); and 300 nm region (**n**) for commercial mannitol (CM), spray dried mannitol (SDM), and freeze dried mannitol (FDM) (mean ± SE, $n \geq 2$).

of detectable amounts of amorphous mannitol and/or mannitol hydrate within all mannitol products, since amorphous mannitol is usually identified by glass transition at about 13°C followed by two crystallization exotherms at about 25°C and 65°C (24). Since α-mannitol and β-mannitol forms are indistinguishable in DSC traces (Table I), all mannitol samples were further analysed using FT-IR (Fig. 5a) and PXRD (Fig. 5b).

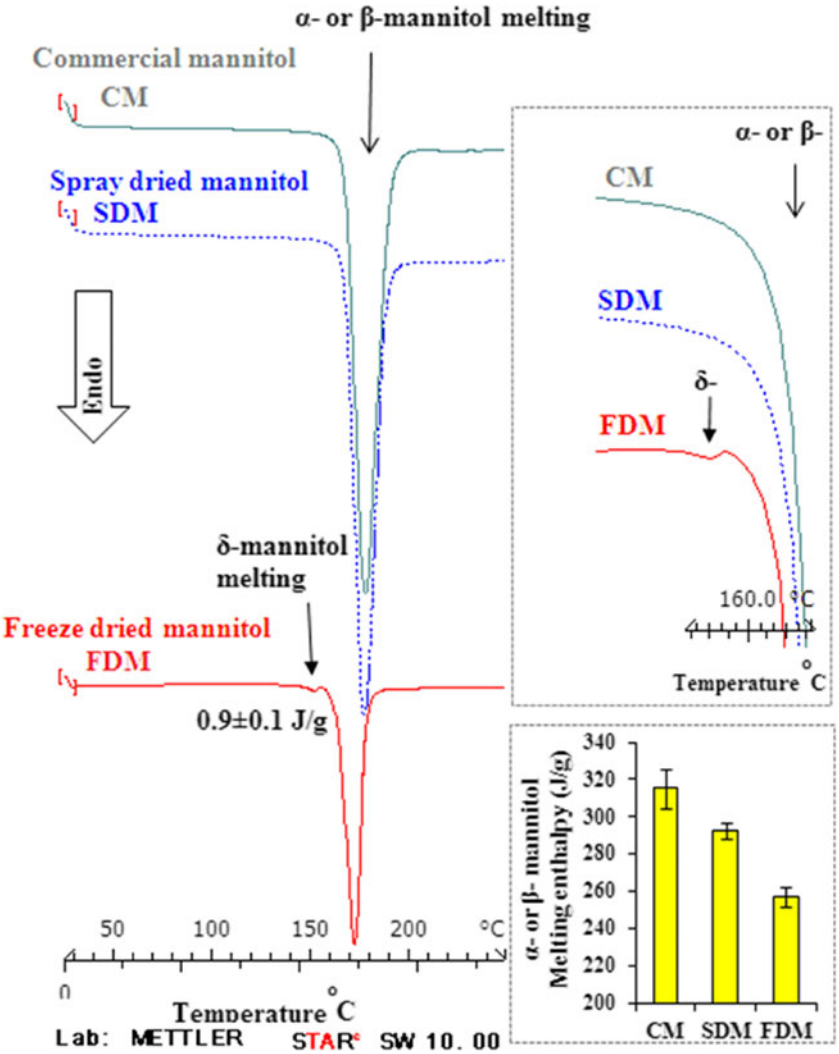

Fig. 4 Differential scanning calorimeter traces and melting enthalpies of commercial mannitol (CM), spray dried mannitol (SDM), and freeze dried mannitol (FDM).

CM exhibited the typical FT-IR spectrum and PXRD pattern for the reference β-mannitol (Table I), having the FT-IR specific diagnostic bands at 929 cm^{-1}, 959 cm^{-1}, and 1,029 cm^{-1} (Fig. 5a) and PXRD diagnostic peaks at 10.6°, 14.7 °, 23.4 °, and 29.5 ° (Fig. 5b). SDM showed the FT-IR distinctive band of α-mannitol (1,194 cm^{-1}), FT-IR specific bands of β-mannitol (929 cm^{-1} and 959 cm^{-1}) (Fig. 5a), PXRD specific peaks of α-mannitol (9.6°, 13.8°, and 17.2°), and PXRD specific peaks of β-mannitol (10.6°, 14.7°, 23.4°, and 29.5°) (Fig. 5b) (Table I). This indicates that SDM consist of mixtures of α-mannitol (~58%, *w/w*) and β-mannitol (~43%, *w/w*) (Fig. 5b). FDM showed the FT-IR specific band

Table I DSC Melting Points, FT-IR Diagnostic Bands, and PXRD Diagnostic Diffraction Angles for: α-mannitol, β-mannitol, and δ-mannitol Polymorphic Forms

Technique	Polymorphic from of mannitol					
	α-	References	β-	References	δ-	References
Melting point (DSC) (°C)	166.0	Yu *et al.* (41)	166.5	Yu *et al.* (41)	150–158	Burger *et al.* (34) Kaialy *et al.* (5,15,33)
Band (FT-IR) (cm^{-1})	1194	Burger *et al.* (34) Kaialy *et al.* (3,4,27)	1209, 959, 929	Burger *et al.* (34) Kaialy *et al.* (3,4,15,27)	967	Burger *et al.* (34) Kaialy *et al.* (4,15,27)
Diffraction angle (PXRD) (°)	9.6, 13.8, 17.2	Burger *et al.* (34) Kaialy *et al.* (4,27)	10.6, 14.7, 23.4, 29.5	Kaialy *et al.* (4) Kaialy *et al.* (15,27)	9.74, 22.2	Burger *et al.* (34) Kaialy *et al.* (4,15,27)

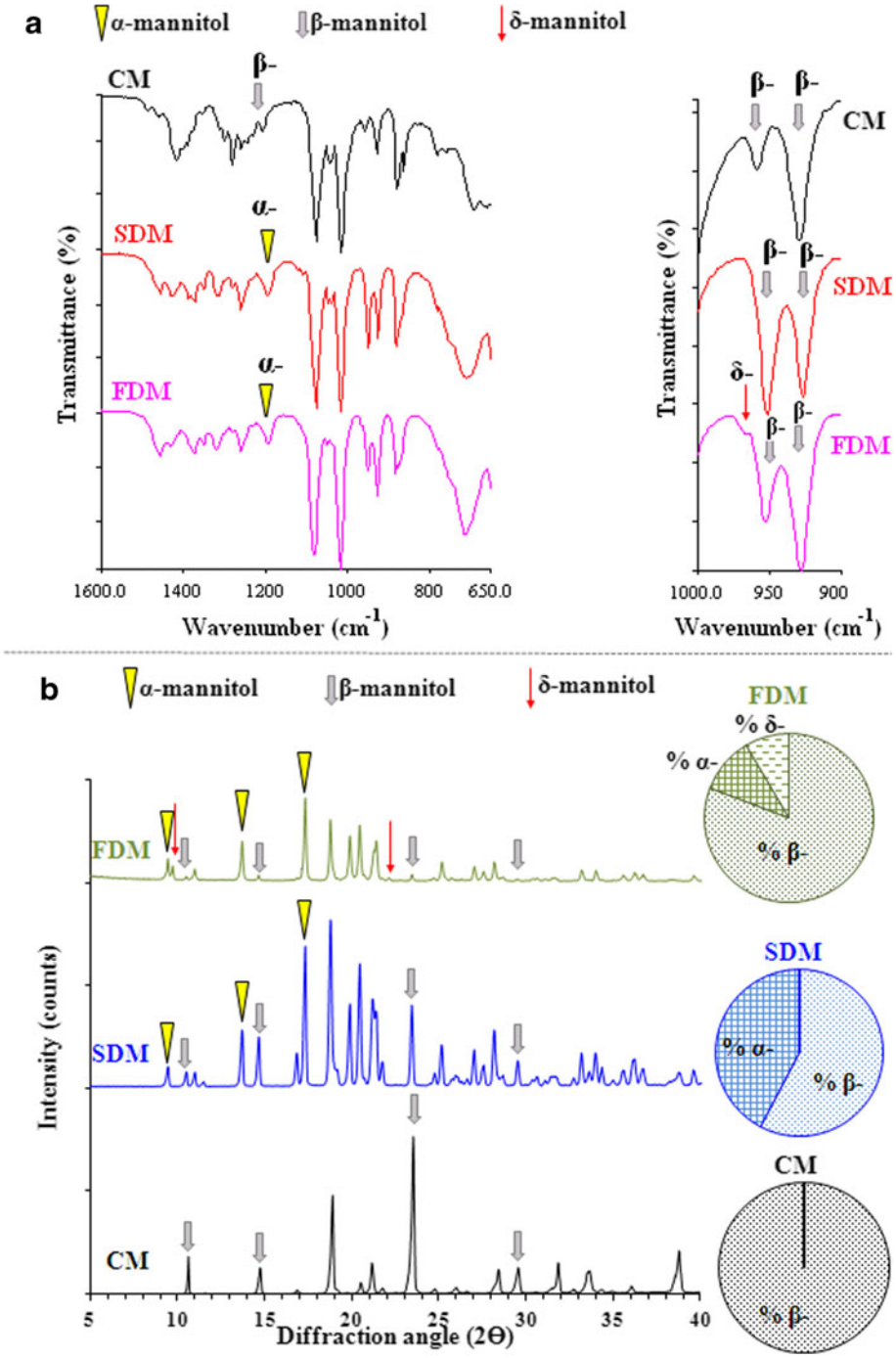

Fig. 5 FT-IR spectra (**a**); and PXRD patterns (**b**) for commercial mannitol (CM), spray dried mannitol (SDM), and freeze dried mannitol (FDM).

of α-mannitol (1,194 cm^{-1}), FT-IR specific band of β-mannitol (929 cm^{-1} and 959 cm^{-1}), FT-IR specific band of δ-mannitol (967 cm^{-1}) (Fig. 5a), PXRD specific peaks of α-mannitol (9.6°, 13.8°, and 17.2°), PXRD specific peaks of β-mannitol (10.6°, 14.7°, 23.4°, and 29.5°), and PXRD specific peaks of δ-mannitol (9.74° and 22.2°) (Fig. 5b) (Table I). This indicates that FDM crystallised as mixtures of α-mannitol (~81%, *w/w*), β-mannitol (~11%, *w/w*), and δ-mannitol (~8%, *w/w*) (Fig. 5b).

High peak resolution of PXRD patterns (Fig. 5b) in addition to DSC thermal traces (Fig. 4) and SEM photos (Fig. 2d–f) confirm the highly crystalline nature of all mannitol products. However, in comparison to CM, decreased DSC melting enthalpy (Fig. 4) and lower PXRD peak intensities (Fig. 5b) for FDM sample suggest its lower relative degree of crystallinity. This might be influenced by the presence of 3.9±0.6% (*v/v*) of $FPM_{<10\mu m}$ in FDM sample (Figs. 1a, 2f), as it is known that finer particles of the same

material have smaller relative degree of crystallinity (9). Also, it is known that δ-mannitol has smaller melting point since it is enantiotropic toward α- and β- forms whereas β-mannitol is monotropic toward α-form (34).

In conclusion, CM product was in β-mannitol form whereas SDM product was mixtures of α- and β-mannitol and FDM sample crystallized as a mixture of α-, β-, and δ-mannitol forms (Table II). Such results indicate the suitability of the applied freeze drying method to prepare crystalline mannitol product. α-, β-, and δ- mannitol polymorphic forms are stable for minimum 5 years in dry atmosphere at 25°C.

It is believed that, during freeze drying, the intra- and inter- hydrogen bonds of D-mannitol are broken by solvents containing hydroxyl group (such as water) inducing crystal form conversion. The presence of δ-mannitol in FDM sample might contribute to the elongated morphology of FDM crystals since both particle shape and unite cell of δ-mannitol is elongated (oblong) (15). Such differences in polymorphic form between different mannitol products is important as it is known that different polymorphs of the same compound could have different physical and chemical properties and may lead to pharmaceutical product with different characteristics (15).

Density and Flowability

CM showed similar true density (particle density) to the value reported in literature for β-D-mannitol (Table II). However, SDM and FDM particles showed different true densities to that of CM (Table II) which could be ascribed to their different molecular configuration induced by their different polymorphic form (Table II; ref. 3,4) and different size (Fig. 1a; ref. 8,9).

Unlike true density (which is particle characteristic), bulk density and tap density are powder characteristics which are indicative of powder packing and compaction properties. Powder porosity refers to the voids within the powder bed including spaces between agglomerates, between primary particles, and micro-spaces (micropores) within the particles.

Table II Polymorphic from, True Density, Bulk Density, Tap Density, Porosity, and Flow Character for Commercial Mannitol, Spray Dried Mannitol, and Freeze Dried Mannitol (mean±SD, $n \geq 4$)

Physical property	Commercial mannitol	Spray dried mannitol	Freeze dried mannitol
Polymorphic form	β-	α-+β-	α-+β-+δ-
True density (g/cm^3)	1.52±0.00	1.45±0.01	1.47±0.01
Bulk density (g/cm^3)	0.54±0.01	0.46±0.00	0.19±0.01
Tap density (g/cm^3)	0.63±0.01	0.53±0.01	0.26±0.01
Porosity (%)	64.5±0.8	68.4±0.2	87.1±0.5
Flow character	Good	Excellent	Poor

SDM powder showed smaller bulk density (apparent density), smaller tap density, and higher porosity than CM (Table II). This might be due to spherical shape and relatively smaller size (8,9) of SDM particles in comparison to CM particles (Figs. 1, 2). Higher bulk density, higher tap density, and smaller porosity for CM powder in comparison to SDM are indicative of relatively increased number of interparticulate contacts between CM particles. Among mannitol powders, FDM powder demonstrated the lowest bulk density, the lowest tap density, and highest porosity (Table II) indicating fewer points of physical contact between particles within FDM powder. This could be attributed to pronounced internal friction (interlocking ability) within FDM powder due to the elongated most irregular (anisometric) shape of FDM particles (Figs. 1e, 2f) resulting in additional void space between particles within FDM powder. Such data suggest that interparticulate cohesive forces between different mannitol powder were in the following rank order: CM>SDM>FDM.

Among mannitol powders, SDM showed the best flow properties (excellent flow character, CI=14.0±0.8%) whereas FDM showed the poorest flow properties (poor flow character, CI=27.2±1.2%) (Fig. 6a). It is believed that spherical shape of SDM particles renders the SDM powder better flowability. Poorer flowability for FDM powder could be ascribed to its more irregular particle shape (Figs. 1e, 2f) which induce pronounced internal friction (geometric interlocking) within FDM powder. Also, the presence of fine particle mannitol in FDM powder (Figs. 1a, 2f) could contribute to its poorer flowability (8,9). Plotting CI of different mannitol powders against mannitol particle sphericity and $FPM_{<10\mu m}$ indicated better flowability in case of mannitol powders with more higher shape sphericity and smaller fines content (Fig. 6b). It is believed that higher fines content (higher $FPM_{<10\mu m}$) and poorer flowability (higher CI) of mannitol powder account for its less homogeneous PSDs (higher span) as evident in Fig. 6c. In fact, mannitol powders with poorer flowability are more difficult to pass through mesh opening during sieving process.

Evaluation of Drug-Carrier Formulations

Drug Content Homogeneity

SS- CM and SS-FDM formulations produced similar ($P>0.05$) potency with values ranging from 89.9±6.0% to 92.0±8.8% of the nominal dose which fall within FDA and USP criteria for content uniformity (85–115%) (Fig. 7a). However, SS-SDM formulation produced considerably smaller potency (78.1±2.5%) which exceed the acceptable range (Fig. 7a). This could be ascribed to spherical shape of SDM particles (Figs. 1d, 2e) which might facilitate "mechanical disconnection" of SS particles adhering on the mannitol surface during formulation powder handling processes (e.g. mixing, vial filling, capsule

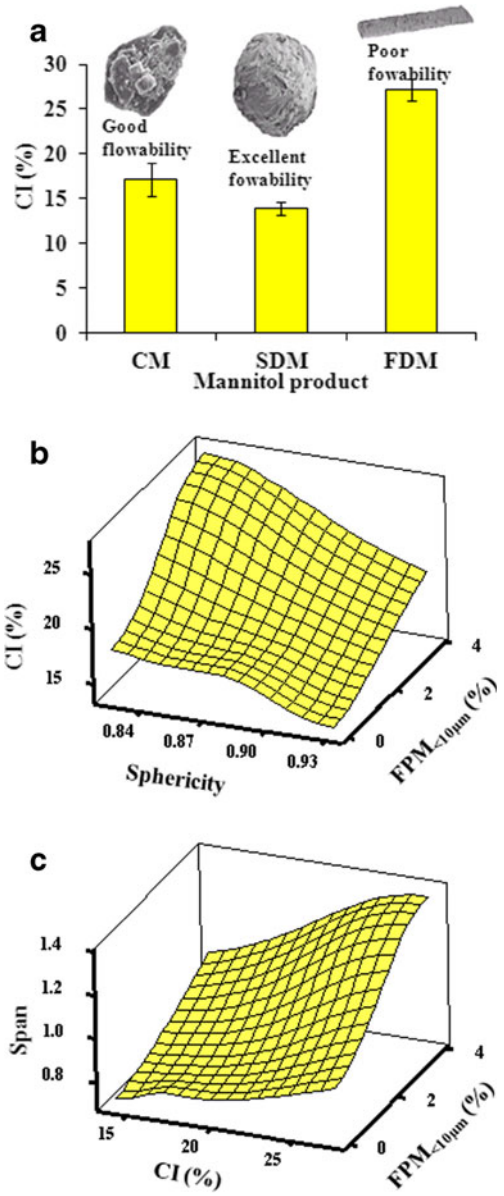

Fig. 6 Carr's index (CI) (**a**); CI in relation to Sphericity and fine particle mannitol ($FPM_{<10\mu m}$) (**b**); and Span in relation to CI and $FPM_{<10\mu m}$ (**c**); for commercial mannitol (CM), spray dried mannitol (SDM), and freeze dried mannitol (FDM) (mean±SD, $n \geq 4$).

filling, etc.) and thus might lead to substantial amount of drug being "lost" on the surface of mixing cylinder, glass vial container, etc.

CV (%) of SS content obtained from different formulations was within the following rank order: SS-SDM<SS- CM<SS-FDM (Fig. 7a). In case of SS-CM and SS-SDM formulations, the % CV of SS distribution was <6%, suggesting that the SS particles were homogeneously distributed throughout the formulation powder mixture. However, FDM generated heterogeneous DPI mixture (least uniform SS content, CV>6%). Poor flowability of FDM powder (Fig. 6a) might contribute to poor homogeneity of SS-FDM formulation (7) since it might affect SS-mannitol blending process. In addition, poor homogeneity of SS-FDM formulation powder could be attributed to higher PSD polydispersity of FMD (Figs. 1b, 2f), which might promote percolation segregation leading to the formation of drug-rich areas (higher amounts of drug per unite mass) within SS-FDM formulation (9). Figure 7b shows that the wider PSD (higher span) and the poorer the mannitol powder flowability (higher CI) the poorer the SS content homogeneity within DPI formulation (higher %CV). Such data indicate that in DPI mixtures, the efficiency of DPI formulation blending and thus achieving uniform stable ordered mixture with homogeneous drug content (and therefore uniform metering doses by the patient) is deeply affected by the flow/size polydispersity properties of the carrier.

Since blending process might have a significant influence on interparticulate interactions within a powder formulation and thus DPI performance (12), no blending-optimization was conducted for each formulation in order to meet the comparison purpose of this study.

Drug-Carrier Adhesion Assessments. In DPIs, drug inhalation behaviour depends on the balance between removal forces (inertial forces: e.g. particle-particle collision and particle-inhaler wall collisions; shear forces: e.g. particle-inhaler wall friction; and lift or drag forces: e.g. forces within turbulent air

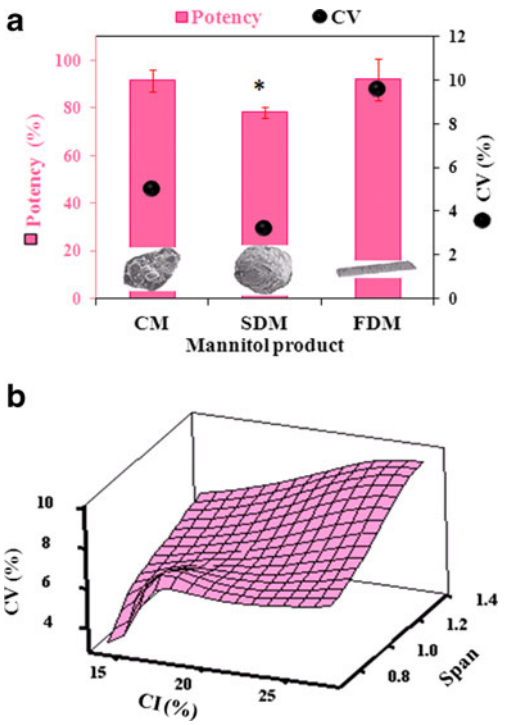

Fig. 7 % Potency (*Pink Square*) and % coefficient of variation (CV) (*Black Circle*) of salbutamol sulphate (SS) content (**a**); and % CV of SS in relation to and Carr's index (CI) and span of mannitol (**b**) for SS-mannitol formulations containing commercial mannitol (CM), spray dried mannitol (SDM), and freeze dried mannitol (FDM) (mean±SD, $n=7$) (*Asterisk* indicates statistically different ($P<0.05$)).

stream) and interaction forces (e.g. Van der wall forces) during inhalation. Air jet sieving could be better than AFM in characterizing drug-carrier interparticulate forces since AFM has the drawback of considering only single particle rather than the overall powder. During air-jet sieving, drug particles are expected to separate from carrier particles. During air jet sieving, particles are submitted to both aspiration (generated by negative pressure) and airflow (generated by the blow nozzle rotating under the sieve). Assuming particle adhesive forces are equivalent to particle removal forces (15), less amount of SS remained in powder on top of the sieve indicate weaker SS-mannitol adhesion. For all formulations, the amounts of drug decreased with increasing the functional sieving time (Fig. 8a). Logarithmic relationships were obtained when plotting amounts of SS remained against sieving time ($r^2 \geq 0.98$, figures not shown) from which $T_{50\%}$ values were calculated defined elsewhere (27) (Fig. 8a). CM produced the highest amounts of SS following all sieving times (Fig. 8a) indicating greatest degree of SS-mannitol adhesive forces. This could be attributed to the larger size of CM particles in comparison to other mannitol particles (Fig. 1a), which is expected to generate higher press-on forces (the forces that press the drug particles onto the carrier particles) during mixing process which acts as adhesive forces (12,15). Also, it can be assumed that detachment of small SS particles from large mannitol particles occurs laterally on the mannitol particle surface (SS particles slip along the mannitol particle surface till they reach the edge and falls off). Therefore, the distance that the drug particles have to slip on mannitol carrier surface increase with particle size of carrier mannitol, thus the greater the aerodynamic drag force (F_{drag}) which plays as adhesive force between SS and mannitol particles.

After all functional sieving times, FDM produced smaller amounts of SS than SDM which in turn produced smaller amounts of SS than CM (Fig. 8a). Such findings indicate that SS particles attached to FDM carrier particle surfaces detached more easily than SS particles adhered to SDM carriers, from which SS drug particles separated more easily in

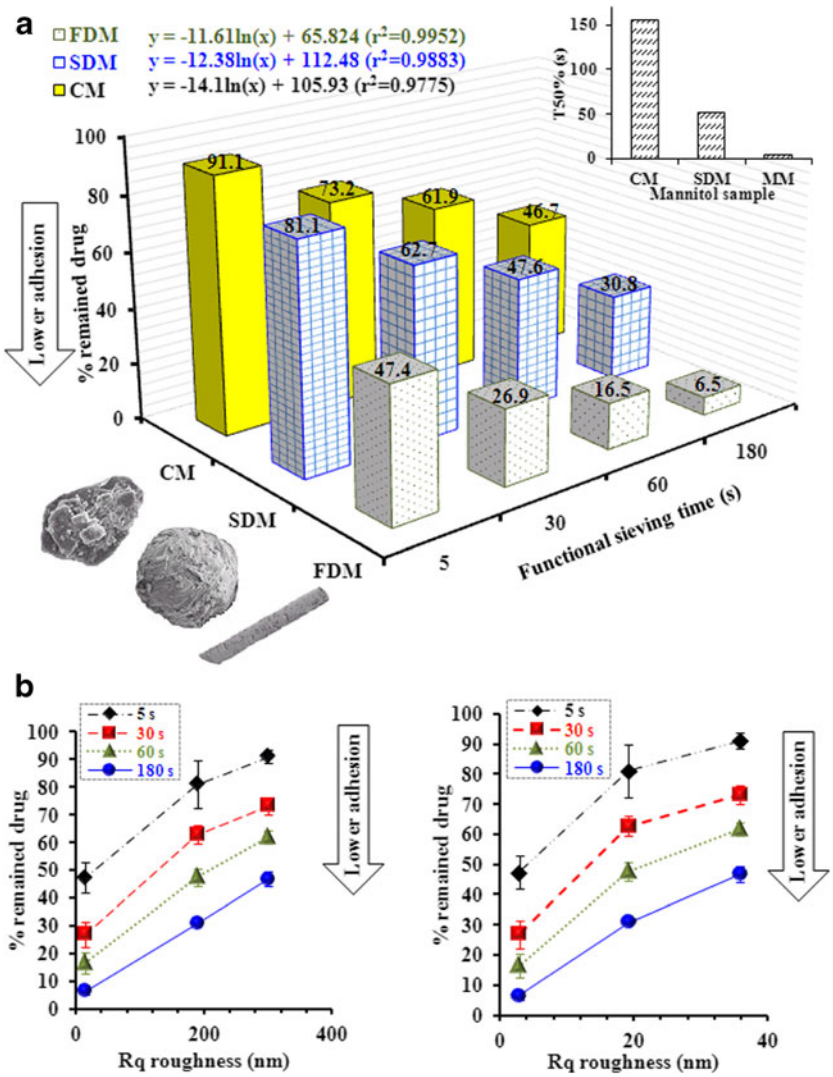

Fig. 8 *Percent* amounts of salbutamol sulphate (SS) remaining on top of the 20 μm sieve and $T_{50\%}$ obtained from formulations containing commercial mannitol (CM), spray dried mannitol (SDM), and freeze dried mannitol (FDM) after different functional sieving times: 5 s (*Black Diamond*), 30 s (*Red Square*), 60 s (*Green Triangle*), and 180 s (*Blue Circle*) (**a**); % remained SS in relation to root mean square average (Rq) roughness on a 5 μm region and 300 nm region of mannitol particle surface (mean±SD, $n \geq 3$) (**b**).

comparison to CM particles. $T_{50\%}$ obtained from different formulations was in the following rank order according to mannitol product: CM (155.5 s)>SDM (52.8 s)>FDM (3.9 s) (Fig. 8a). This confirms that SS-mannitol adhesive forces within different formulations were within the following hierarchy according to mannitol product: $F_{CM}>F_{SDM}>F_{FDM}$ (Fig. 8a). Deceased drug-carrier adhesive forces in case of FDM could be attributed to the existence of fine mannitol particles (Figs. 1a, 2f), increased particle shape irregularity (Fig. 2), and/or the smoother particle surface (Fig. 3) in the case of FDM, all of which can contribute to reduced contact area between SS particles and mannitol particles (increased separation distance) and decreased push-on forces (12,27,35). On the other hand, SS particles adhered in a deep concavity on mannitol surface, as in case of CM (Fig. 3), would become entrapped and relatively immobile in the macroscopic depressions.

Fine mannitol particles are proposed to contribute to weak drug-carrier adhesion by saturation of "active sites" (high adhesion sites) on the coarse mannitol particles, which leaves the passive sites (low adhesion sites) available for SS adhesion. Also, it can be assumed that fine mannitol particles physically disrupt the SS-mannitol contacts leading to smaller SS-mannitol adhesion. Moreover, based on "agglomeration theory" (7,10), the presence of fine particle mannitol in FDM sample (Fig. 2f) could promote the formation of SS-fine mannitol mixed agglomerates. These agglomerates are expected to be e easier to detach from carrier surface upon inhalation than single SS particles. It is believed that SS-fine mannitol mixed agglomerates might form at the expense of SS-coarse mannitol ordered mixtures (interactive mixtures), and this leads to the reduction of amounts of single SS particles attached to larger mannitol particles and thus smaller SS-mannitol total adhesion (Fig. 8a).

The adhesion of particles is a surface phenomenon and therefore, the drug-carrier adhesion is deeply affected by the surface morphology of both carrier particles and drug particles. The existence of different surface morphologies (disturbance on the crystal surface) between different mannitol particles is likely to result in different physicochemical properties including different "adhesive potential". Fig. 8b shows that the smoother the mannitol particle surfaces (on both 5 μm and 300 nm mannitol surface region) the weaker the drug-carrier adhesive forces. This could be ascribed to lower contact area and thus lower adhesive forces between the adjacent drug particles and carrier particles with smoother surface topography (36). Also, it can be assumed that the use of carrier particles with smoother surfaces could be related to a less binding sites with multiple contact points (10,37). It has been suggested that the rougher the carrier particles, the greater number of active sites which are capable of binding the drug particles more strongly and as a result the higher proportion of drug adhering to the carrier particles (38). Decreased SS-mannitol adhesion in case of SS-FDM (Fig. 8a) formulation might contribute to easier segregation of SS from mannitol surfaces and thus poor content homogeneity of SS within SS-FDM formulation (Fig. 7a).

In Vitro Aerosolization Performance. Stage by stage mass distribution deposition profiles of SS varied considerably according to the type of mannitol product (Fig. 9a). Amounts of SS adhered to inhaler wall with mouthpiece adaptor (residual drug, drug loss, or device retention) ranged from 3.7±0.2% to 6.2±5.8% (Fig. 9a). Such amounts could be attributed to electrostatic attraction. Also, it can be assumed that SS particles detach from mannitol surfaces within the inhaler device. FDM deposited considerably ($P>0.05$) higher amounts of SS on throat (9.8±0.6%) in comparison to CM and SDM (3.0±0.7%) (Fig. 9a). This could be attributed to the presence of fine particle mannitol ($FPM_{<10\mu m}$) (Figs. 1a, 2f) and poor flowability (Fig. 6a) in case of FDM powder, which promote the formation of $FPM_{<10\mu m}$-$FPM_{<10\mu m}$ and $FPM_{<10\mu m}$-SS agglomerates depositing on throat by inertial impaction (7,39), especially when using low resistance device such as Aerolizer® being used in this study (40). Amounts of drug deposited on I&M and IP are believed to be eventually swallowed and consequently systemically absorbed via the GIT (Fig. 9a).

In case of SS-CM and SS-SDM aerosol formulations, SS particles deposited preferentially on stage 1 (cut off diameter= 10.5 μm) representing the upper airways (tracheobronchial deposition) (Fig. 9a). However, SS-FDM aerosol formulation exhibited maximal deposition on stages: 2 (representing bronchial airways), 3 (representing peripheral alveolar airways), and 4 (representing deep lung airways) with no substantial difference between these stages (19.2±2.3–23.8±2.7%, $P>0.05$) (Fig. 9a). All aerosol formulations exhibited minimal deposition on MsLI-filter with FDM generating significantly higher amounts of SS than CM (Fig. 9a). The aerodynamic PSD of SS analyzed by MsLI as obtained from different SS-mannitol aerosol formulations is shown in Fig. 9b. All SS-mannitol aerosol formulations generated linear log aerodynamic PSD plots ($r^2\geq0.904$) confirming the absence of particle bounces and re-entrainment during aerosolization (Fig. 9b). The slops of these aerodynamic PSD linear regressions was named as constant K, which could be used as a parameter to indicate DPI performance (9,14). In determining aerosol PSD, aerodynamic size is more suitable than geometric size. When compared to geometric particle size (raw SS powder before aerosolization, measured by laser diffraction, K=92.9), SS-mannitol aerosol formulations generated larger aerodynamic size distributions (after aerosolization, analysed by MsLI, K= 21.2–58.9) (Fig. 9b). This indicates that SS particles were not sufficiently dispersed during inhalation to recover the primary (individual) particles. This could be caused by insufficient SS-SS deagglomeration (high SS-SS cohesive forces) and/or

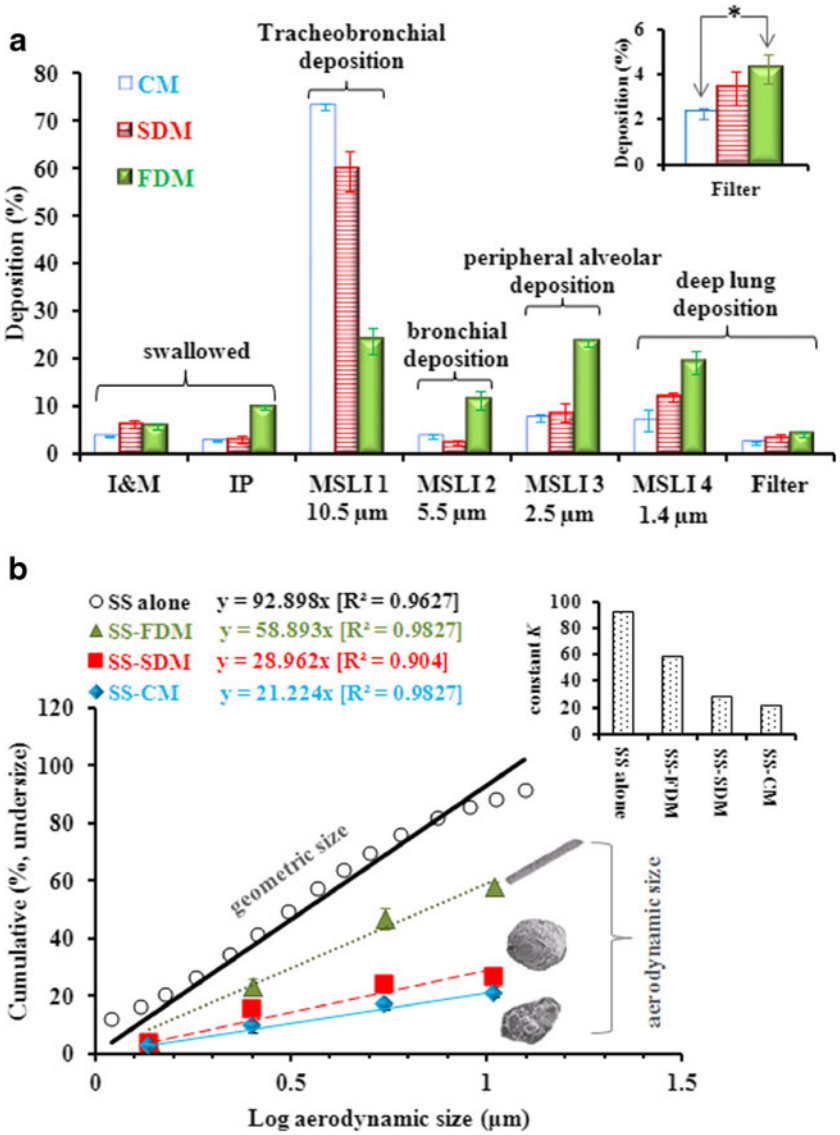

Fig. 9 Amounts of salbutamol sulphate (SS) deposited on inhaler plus mouthpiece adaptor (I&M), induction port (IP), and different MsLI stages (**a**); (*White Circle*) geometric particle size (before aerosolization) and aerodynamic particle size (after aerosolization) of SS obtained from formulations containing commercial mannitol (CM) (*Blue Diamond*), spray dried mannitol (SDM) (*Red Square*), and freeze dried mannitol (FDM) (*Green Triangle*) (**b**).(mean ± SD, $n=3$). (*Asterisk* indicates statistically different: $P < 0.05$).

Table III Recovered Dose (RD), Emitted Dose (ED), Mass Median Aerodynamic Diameter (MMAD), Geometric Standard Deviation (GSD), Fine Particle Dose (FPD), Impaction Loss (IL), Fine Particle Fraction (FPF), and Dispersibility (DS) of Salbutamol Sulphate Obtained from Formulations Containing Commercial Mannitol, Spray Dried Mannitol, and Freeze Dried Mannitol (mean ± SD, $n=3$)

Deposition parameter	Commercial mannitol	Spray dried mannitol	Freeze dried mannitol
RD (µg)	381.5 ± 8.3	394.2 ± 23.9	465.9 ± 8.2
ED (µg)	367.3 ± 8.8	350.6 ± 26.6	428.1 ± 4.9
MMAD (µm)	3.0 ± 0.2	2.6 ± 0.1	3.2 ± 0.2
GSD	2.2 ± 0.0	2.2 ± 0.0	2.1 ± 0.1
FPD (µg)	64.3 ± 6.5	94.6 ± 14.4	218.6 ± 20.3
IL (%)	75.7 ± 0.7	62.6 ± 3.6	33.6 ± 2.3
FPF (%)	16.8 ± 1.3	24.0 ± 2.7	46.9 ± 3.6
DS (%)	17.5 ± 1.4	17.5 ± 1.4	26.9 ± 2.6

insufficient SS-mannitol deaggregation and/or inadequate dispersing efficiency of the inhaler device.

The aerodynamic PSD of SS particles generated from SS-FDM formulations ($K=58.9$) was closer to the primary PSD of pure SS powder than that of the aerodynamic PSD generated from SS-SDM formulations ($K=29.0$) which in turn generated smaller aerodynamic PSD than SS-CM formulations ($K=21.2$) (Fig. 9b). This indicates that FDM generated smaller aerodynamic size of SS than SDM which in turn generated smaller aerodynamic size of SS than CM upon aerosolization. FDM deposited larger proportion of SS dose to the central and lower airways (or the impactor) than SDM from which SS particles are expected to reach lower airway regions (which are the site of action in case of SS) in comparison to SS particles formulated with CM carrier.

Apart from *in vivo* lung drug dose or drug safety, RD and ED are considered important quality control indicators of pharmaceutical performance. The RD of SS obtained from

all formulations was within the range between 381.5±8.3 μg and 465.9±8.2 μg corresponding to % recovery between 79.3±1.7% and 96.9±1.7%, which is within the acceptable range of % recovery (75–125%) (Table III), supporting the highly dispersible nature of all mannitol powders. Also, this suggests good reproducibility and reliability of the overall procedures including mixing, sampling, capsule filling, deposition, washing and the analysis of SS were satisfactory accurate. FDM generated higher RD and higher ED of SS than other mannitol products (Table III) indicating higher dose of SS available to the patient or the impactor when delivered from the inhaler device. Upon aerosolisation, the formulation powder is forced out from the capsules through the pierces and pulled into the oral cavity by the drag forces exerted upon the particles generated from the airflow. High RD and ED in case of SS-FDM formulation reflect the appropriate aerodynamic properties of FDM powder and could be ascribed to reduced protuberances on FDM particle surface (Fig. 3) which may reduce the SS-mannitol geometrical interlocking leading to improved SS-mannitol deaggregation within the inhaler device during aerosolization. On the other hand, smaller RD and RD in case of CM and SDM could be ascribed to their higher bulk density (Table II), since it is known that cohesive powders are more difficult to fluidize via airflow (lift as fractures or plugs) than less cohesive powders, such as FDM (Table II), which fluidize more homogeneously by an erosion mechanism.

A MMAD in the range of 1–5 μm is very important to achieve efficient pulmonary drug delivery. In this study, MMAD of SS ranged between 2.6±0.1 μm and 3.2±0.2 μm with GSD of 2.2±0.1 indicating polydisperse (or heterodisperse) PSD of aerosolized SS (GSD>1.2) (Table III). Although the same batch of SS was used in preparation of all formulations, SDM generated smaller MMAD of SS in comparison than CM and FDM (Table III) indicating smaller drug agglomeration. The presence of fine particle mannitol in case of FDM (Figs. 1a, 2f) might account for increased MMAD in case of SS-FDM in comparison to SS-SDM due to the formation of SS-FDM$_{<10\mu m}$ aggregates (7). Also, rougher surface of CM (Fig. 3) might contribute to higher MMAD in case of SS-CM in comparison to SS-SDM (10). In theory, judging from geometric and aerodynamic particle size of SS (Fig. 9b), all SS particles are supposed to deposit on lower stages of the MsLI. However, IL of SS ranged between 33.6±2.3% (SS-FDM) and 75.7±07% (SS-CM) (Table III). This indicates that the operating flow was not sufficient to generate enough energy input generated by the air stream through the devise and thus not all of SS particles has detached from mannitol surfaces. By examining only the MMAD values (Table III), it might be thought that SS-SDM formulation would demonstrate the best aerosolisation efficiency across other formulations. However; the following rank order could be formulated for FPD, FPF, and DS obtained from different formulations according to mannitol product: CM<SDM<FDM (Table III) whereas the reverse order could be observed in respect to IL (Table III). Drug-carrier aerosolization performance is, mainly, dependent on two factors: 1) drug-drug cohesion forces (drug-drug self agglomeration which is reflected by MMAD) and 2) drug-carrier adhesion forces (drug- coarse carrier aggregation). In fact, smallest MMAD obtained for SS-SDM formulation indicate smallest degree of SS-SS cohesion (SS self agglomeration) but it does not mean necessarily smallest degree of SS-SDM adhesion (SS-SDM aggregation), which is proved by drug-carrier adhesion assessments (Fig. 8). Depending on the drug-drug cohesion and drug-carrier adhesion balance, formulations with lower MMAD still can produce higher FPF and *vice versa* (7–9).

Wider variation in FPF in the case of SS-FDM (SD=3.6), in comparison to SS-CM (SD=1.3) and SS-SDM (SD=2.7) formulations (Table III), could be related to poorer drug content homogeneity of SS-FDM formulation in comparison to other formulations (Fig. 7a). It is clear that FDM generated ~2.8 fold larger FPF than CM and ~2.0 fold increase in FPF than SDM. This indicates that SS particles attached to elongated-FDM were easier to disperse than SS particles attached to spherical-SDM from which SS particles were easier to disperse than angular-CM. This confirms superior DPI performance of FDM since it is known that higher FPF does not only indicate enhanced therapeutic efficiency and a decrease in the dosage required for asthma treatment, but also a minimized side effects and a promoted patient compliance. It is believed that the SS-FDM formulation presented in this study showed the best aerosolization performance of SS reported in literature so far (fine particle fraction of 47% and dispersibility of 51%, in the case of SS-carrier DPI formations with 63–90 carrier particles, <5 μm drug particles, Aerolizer® inhaler device, flow rate of 92 L/min, and 67.5:1 (*w*/*w*) drug-carrier ratio). This suggests that FDM powder may even be considered in aerosol formulations for local and systemic drug delivery.

Since all formulations were prepared under similar protocols, differences in aerosolization performance between different SS-mannitol aerosol formulations may be attributed to different mannitol products. Regression analysis showed that the aerosolization performance obtained from different SS-mannitol formulations demonstrated poor relationships with VMD, aspect ratio, flakiness ratio, sphericity, simplified shape factor, and Carr's index of mannitol. This suggests that, at least within data in this study, there is no simple apparent relationship between size, shape, and/or flowability of mannitol and *in vitro* aerosolization performance of SS. In fact, the effect of carrier particle size, shape, and flowability as one variable on drug aerosolisation efficiency from DPIs was reported in contrary manner as explained previously. However, Both FPF and IL exhibited good relationship with $T_{50\%}$ (Fig. 10a) indicating that the weaker the SS-mannitol adhesive

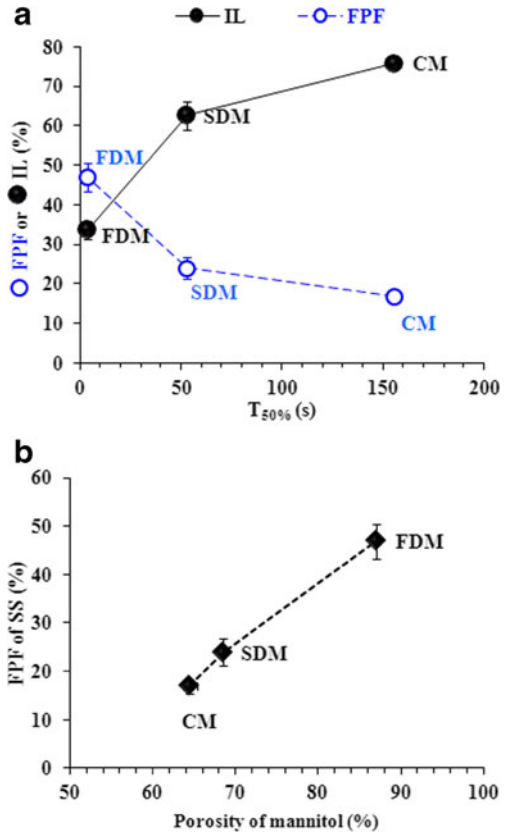

Fig. 10 Fine particle fraction (FPF) (*White Blue Circle*), impaction loss (IL) (*Black Circle*) of salbutamol sulphate (SS) (**a**); and FPF of SS in relation to porosity of mannitol powder (*Black Diamond*) (**b**) obtained from formulations containing commercial mannitol (CM), spray dried mannitol (SDM), and freeze dried mannitol (FDM).

forces the smaller the amounts of SS attached to the carrier following aerosolization and the increased amounts of drug delivered to lower airways.

During inhalation, two main mechanisms are believed to control SS-mannitol detachment : detachment by the flow stream (flow detachment, fluid forces) and detachment by impaction (mechanical detachment, mechanical forces). In the case of SS-FDM formulation, detachment by flow is expected to be the dominate mechanism, since such detachment dominates in the case of smooth surface–carrier particles (Fig. 3). However, detachment by mechanical forces is believed to be more relevant is case of SS-CM formulation since such detachment relies on the abrupt momentum transfer resulting from particle-inhaler collisions and it is facilitated for carrier particles with rougher surfaces (Fig. 3) (16).

It should be acknowledged that particles with lower density are more advantageous for inhalation due to their smaller aerodynamic diameter in comparison to their geometric diameter. The use of particles with smaller density is likely to lead to reduced probability of deposition by inertial impaction and sedimentation (increased residence time). It is believed that, in determining aerosol PSD, particle aerodynamic size is more suitable than geometric size. Despite that SDM and FDM particles have similar geometric diameter (Fig. 1b), they demonstrated considerably different aerodynamic diameters: 59.9 $\pm$0.8 μm and 41.3$\pm$0.6 μm for SDM and FDM respectively. Superior DPI performance of FDM in comparison to SDM could be attributed to smaller density and higher porosity of FDM powder (Table II) which gives rise FDM powder smaller interparticulate cohesive forces in dry state and reduced setting velocity in aerosolized state (more airborne) promoting deeper penetration in lung airways. By comparing different formulations, the higher the mannitol powder porosity the higher are the amounts of drug delivered to lower airway regions (Fig. 10b). It can be suggested that mannitol particle physical properties (e.g. morphology) manipulate fine particle delivery to lower airway regions due to their effect on powder bulk properties. Interactions between SS particles, SS agglomerates, SS-$FDM_{<10\mu m}$ mixed agglomerates, and SS-mannitol ordered units with single- or multi-SS particles could be impacted by the space size between carrier particles, as supported by percolation theory (40). It is believed that the higher the porosity of the carrier powder the easier is the powder dispersion (segregation) upon aerosolization and the smaller the inertial forces will be generated during aerosolization leading higher aerosol mass deposited on lower airway regions (since the inertial impaction is the predominant deposition mechanism in the lungs). On the other hand, powders with smaller porosity have higher interparticulate forces due to increased number of contact points. These forces must be overcome to produce a dispersed aerosol powder upon inhalation. Therefore, excessive cohesive forces might results in poor dispersion properties because of enhanced particle aggregation which in turn decreases particle fluidization. Finally, it was noted that solid state, size, and aerosolization performance of different mannitol products has not significantly changed following being stored in ambient conditions (22$\pm$1°C, 50% RH) for 6 months (data not shown). Additional systemic stability studies should be performed at elevated temperature and humidity conditions to evaluate variations in physicochemical and inhalation performance of freeze dried mannitol.

Although different mannitol products showed different aerosolization performance, there remain substantial uncertainties regarding carrier functionality in DPI formulations. The theories by which carrier physical properties control DPI performance remain speculative. Full understanding of the relationship between carrier physical properties and DPI performance is still challenging considering the heterogeneous nature of the carriers used in different studies and the high possibility of interaction between different carrier parameters. Although the benefits of using freeze dried mannitol in dry powder aerosol formulation is clear, more efforts would be warranted to comprehensively evaluate the aerosolization performance of freeze dried mannitol with wider range of drug particles, inhalers, and inhalation flow rates. Also, *in vivo*

aerosolization performance assessments would be required to verify if *in vitro* deposition data correlate well with *in vivo* deposition data which is necessary to confirm the use of freezing drying of mannitol as a robust and reliable means of improving aerosolization performance of dry powder inhalers.

CONCLUSION

The work proposed is novel in that it demonstrates another example of the potential of using freeze drying technique in pharmaceutical industry to prepare freeze dried mannitol powders that displayed improved aerosolization performance of salbutamol sulphate from dry powder inhaler formulations. Freeze dried mannitol product was shown to be virtually in complete crystalline nature. For the first time, it was shown that freeze dried mannitol (elongated shape, α-+β-+δ- polymorphic form) produce better aerosolization performance than spray dried mannitol (spherical shape, α-+β- polymorphic form) which in turn demonstrated better aerosolization performance than commercial mannitol (angular shape, β- polymorphic form).

In comparison to commercial mannitol and spray dried mannitol, freeze dried mannitol showed the highest variability in terms of size, shape, solid state, dose homogeneity, and fine particle fraction. Freeze dried mannitol did not show smaller geometric size than spray dried mannitol, however, demonstrated the highest powder porosity. Freeze dried mannitol demonstrated smoother surface morphology than spray dried mannitol which in turn demonstrated smoother surface morphology than commercial mannitol. Freeze dried mannitol generated the weakest salbutamol sulphate-mannitol adhesive forces whereas commercial mannitol generated the highest SS-mannitol adhesive forces. It was clear that the smoother the mannitol surface the weaker the salbutamol sulphate-mannitol adhesive forces.

Among angular, spherical, and elongated shaped mannitol particles, formulators can anticipate better drug delivery to the lung in case of elongated shape mannitol. No apparent relationship was obtained between fine particle fraction and mannitol size, shape, or flowability descriptors. However, mannitol products with higher powder porosity and weaker salbutamol sulphate-mannitol adhesive forces produced higher fine particle fraction of salbutamol sulphate. It was suggested that porosity of carrier powder is an important physical property which can be considered as a key optimization parameter which might be predictive of *in vitro* aerosolization performance of dry powder inhaler formulations.

Mannitol powders with poorer flowability and higher fines content demonstrated wider particle size distributions following sieving. Mannitol powders with less spherical particle shape and higher fines content demonstrated poorer flow properties. Better drug content homogeneity was obtained in case of mannitol powders with better flow properties and narrower size distributions.

Freeze drying of aqueous mannitol solutions is an attractive approach to prepare dry powder aerosol formulations due to its several advantages including enhanced pulmonary drug delivery, maximal yield, simple, low cost effective, and low safety risk, since no organic solvents were used. The use of freeze drying technique can constitute an important step used in the pharmaceutical industry towards preparing freeze dried carrier particles which could help to solve some problems connected to drug-carrier dry powder aerosol formulations.

ACKNOWLEDGMENTS AND DISCLOSURES

Waseem Kaialy thanks Dr. Ian Slipper (University of Greenwich) and Mr. Ian Brown (University of Kent) for help provided with SEM and AFM analysis respectively.

REFERENCES

1. Blagden N, De Matas M, Gavan P, York P. Crystal engineering of active pharmaceutical ingredients to improve solubility and dissolution rates. Adv Drug Deliv Rev. 2007;59:617–30.
2. Aquino R, Prota L, Auriemma G, Santoro A, Mencherini T, Colombo G, Russo P. Dry powder inhalers of gentamicin and leucine: formulation parameters, aerosol performance and *in vitro* toxicity on CuFi1 cells. Int J Pharm. 2012;426:100–7.
3. Kaialy W, Martin GP, Ticehurst MD, Momin MN, Nokhodchi A. The enhanced aerosol performance of salbutamol from dry powders containing engineered mannitol as excipient. Int J Pharm. 2010; 392:178–88.
4. Kaialy W, Momin MN, Ticehurst MD, Murphy J, Nokhodchi A. Engineered mannitol as an alternative carrier to enhance deep lung penetration of salbutamol sulphate from dry powder inhaler. Colloid Surf B. 2010;79:345–56.
5. Kaialy W, Martin GP, Ticehurst MD, Royall P, Mohammad MA, Murphy J, Nokhodchi A. Characterisation and deposition studies of recrystallised lactose from binary mixtures of ethanol/butanol for improved drug delivery from dry powder inhalers. AAPS J. 2011;13:30–43.
6. Kaialy W, Ticehurst MD, Murphy J, Nokhodchi A. Improved aerosolization performance of salbutamol sulfate formulated with lactose crystallized from binary mixtures of ethanol—acetone. J Pharm Sci. 2011;100:2665–84.
7. Kaialy W, Martin GP, Larhrib H, Ticehurst MD, Kolosionek E, Nokhodchi A. The influence of physical properties and morphology of crystallised lactose on delivery of salbutamol sulphate from dry powder inhalers. Colloid Surf B. 2012;89:29–39.
8. Nokhodchi A, Kaialy W, Ticehurst MD. The influence of particle physicochemical properties on delivery of drugs by dry powder inhalers to the lung. In: Popescu MA, editor. Drug delivery book. NY: Hauppauge: Nova; 2011. p. 1–50.
9. Kaialy W, Alhalaweh A, Velaga SP, Nokhodchi A. Influence of lactose carrier particle size on the aerosol performance of budesonide from a dry powder inhaler. Powder Technol. 2012;227:74–85.
10. Podczeck F. The relationship between physical properties of lactose monohydrate and the aerodynamic behaviour of adhered drug particles. Int J Pharm. 1998;160:119–30.

11. Steckel H, Markefka P, TeWierik H, Kammelar R. Effect of milling and sieving on functionality of dry powder inhalation products. Int J Pharm. 2006;309:51–9.
12. Dickhoff B, De Boer A, Lambregts D, Frijlink H. The effect of carrier surface and bulk properties on drug particle detachment from crystalline lactose carrier particles during inhalation, as function of carrier payload and mixing time. Eur J Pharm Biopharm. 2003;56:291–302.
13. Donovan MJ, Smyth HDC. Influence of size and surface roughness of large lactose carrier particles in dry powder inhaler formulations. Int J Pharm. 2010;402:1–9.
14. Kaialy W, Alhalaweh A, Velaga SP, Nokhodchi A. Effect of carrier particle shape on dry powder inhaler performance. Int J Pharm. 2011;421:12–23.
15. Kaialy W, Larhrib H, Ticehurst MD, Nokhodchi A. Influence of batch cooling crystallization on mannitol physical properties and drug dispersion from dry powder inhalers. Cryst Growth Des. 2012;12:300–3017.
16. Le VNP, Thi THH, Robins E, Flament M. Dry powder inhalers: Study of the parameters influencing adhesion and dispersion of fluticasone propionate. AAPS PharmSciTech. 2012;13:477–84.
17. Traini D, Young PM, Thielmann F, Acharya M. The influence of lactose pseudopolymorphic form on salbutamol Sulfate–Lactose interactions in DPI formulations. Drug Dev Ind Pharm. 2008;34:992–1001.
18. Byron PR, Jashnam R. Efficiency of aerosolization from dry powder blends of terbutaline sulfate and lactose NF with different particle-size distributions. Pharm Res. 1990;7:881.
19. Donovan MJ, Kim SH, Raman V, Smyth HD. Dry powder inhaler device influence on carrier particle performance. J Pharm Sci. 2012;101:1097–107.
20. Shur J, Harris H, Jones MD, Kaerger JS, Price R. The role of fines in the modification of the fluidization and dispersion mechanism within dry powder inhaler formulations. Pharm Res. 2008;25:1631–40.
21. Zeng XM, Martin GP, Marriott C, Pritchard J. Lactose as a carrier in dry powder formulations: the influence of surface characteristics on drug delivery. J Pharm Sci. 2001;90:1424–34.
22. Schneid S, Riegger X, Gieseler H. Influence of common excipients on the crystalline modification of freeze-dried mannitol. Pharm Technol. 2008;3:32.
23. Takada A, Nail SL, Yonese M. Influence of ethanol on physical state of freeze-dried mannitol. Pharm Res. 2009;26:1112–20.
24. Hottot A, Nakagawa K, Andrieu J. Effect of ultrasound-controlled nucleation on structural and morphological properties of freeze-dried mannitol solutions. Chem Eng Res Design. 2008;86:193–200.
25. Kim AI, Akers MJ, Nail SL. The physical state of mannitol after freeze–drying: effects of mannitol concentration, freezing rate, and a noncrystallizing cosolute. J Pharm Sci. 1998;87:931–5.
26. Kaialy W, Ticehurst MD, Nokhodchi A. Dry powder inhalers: mechanistic evaluation of lactose formulations containing salbutamol sulphate. Int J Pharm. 2012;423:184–94.
27. Kaialy W, Larhrib H, Martin GP, Nokhodchi A. The effect of engineered mannitol-lactose mixture on dry powder inhaler performance. Pharm Res. 2012;29:2139–56.
28. Krumbein WC. Measurement and geological significance of shape and roundness of sedimentary particles. J Sediment Res. 1941;11:64–72.
29. Fronczek FR, Kamel HN, Slattery M. Three polymorphs (α, β, and δ) of D-mannitol at 100 K. Acta Crystallogr. 2003;59:567–70.
30. Hinds WC. Aerosol technology: properties, behavior and measurement of airborne particles. New York: Jennings: Wiley; 1982.
31. Edwards DA. Delivery of biological agents by aerosols. AIChE J. 2002;48:2–6.
32. Hickey AJ. Pharmaceutical inhalation aerosol technology. New York: Marcel Dekker; 2004.
33. Ho R, Wilson DA, Heng JYY. Crystal habits and the variation in surface energy heterogeneity. Cryst Growth Des. 2009;9:4907–11.
34. Burger A, Henck JO, Hetz S, Rollinger JM, Weissnicht AA, Stöttner H. Energy/temperature diagram and compression behavior of the polymorphs of D-mannitol. J Pharm Sci. 2000;89:457–68.
35. Le VNP, Bierend H, Robins E, Steckel H, Flament MP. Influence of the lactose grade within dry powder formulations of fluticasone propionate and terbutaline sulphate. Int J Pharm. 2011;422:75–82.
36. Ganderton D. The generation of respirable clouds from coarse powder aggregates. J Biopharm Sci. 1992;3:101–5.
37. Kassem NM, Ganderton D. The influence of carrier surface on the characteristics of inspirable powder aerosols. J Pharm Pharmacol. 1990;42(11).
38. Staniforth JN, Rees JE, Lai FK, Hersey JA. Interparticle forces in binary and ternary ordered powder mixes. J Pharm Pharmacol. 1982;34(3):141–5.
39. Le V, Robins E, Flament M. Agglomerate behaviour of fluticasone propionate within dry powder inhaler formulations. Eur J Pharm Biopharm. 2012;80:596–603.
40. Dunbar CA, Hickey AJ, Holzner P. Dispersion and characterization of pharmaceutical dry powder aerosols. Kona. 1998;16:7–45.
41. Yu L, Mishra DS, Rigsbee DR. Determination of the glass properties of D–mannitol using sorbitol as an impurity. J Pharm Sci. 1998;87:774–7.